Evidence that Interaction with the Spacecraft Plasma Wake Generates Plasma Waves Close to the Electron Cyclotron Frequency in the Near-Sun Solar Wind

David M. Malaspina[1,2] , Sabrina F. Tigik[3] , and Andris Vaivads[3]
[1] Astrophysical and Planetary Sciences Department, University of Colorado, Boulder, CO, USA; David.Malaspina@colorado.edu
[2] Laboratory for Atmospheric and Space Physics, University of Colorado, Boulder, CO, USA
[3] Space Plasma Physics, Electrical Engineering and Computer Science, KTH Royal Institute of Technology, Stockholm, 11428, Sweden

Abstract

Prior observations of the near-Sun solar wind (sunward of 0.25 au) identified frequent, intense plasma waves near the local electron cyclotron frequency (f_{ce}), and its harmonics. In this Letter, it is shown that near-f_{ce} wave properties are consistent with generation via interaction between the observing spacecraft's ion wake and the ambient plasma and magnetic fields. This result implies that many observed near-f_{ce} waves are not intrinsic to the unobstructed solar wind flow, and therefore are unlikely to play a significant role in the dynamic evolution of particle distributions in the solar wind.

Unified Astronomy Thesaurus concepts: Solar wind (1534); Space vehicles (1549); Space plasmas (1544)

1. Introduction

Plasma waves are an integral part of the evolving solar wind. Alfvén waves transmit energy from coronal magnetic field motions into the solar wind, and the turbulent dissipation of this energy is expected to play a large role in the heating and/or acceleration of the solar wind (see Smith & Vasquez 2021 for a review). Whistler-mode wave growth and particle scattering may act to regulate the solar electron heat flux (Vasko et al. 2019 and references therein). Langmuir waves, driven by solar-origin electron beams, produce the strongest radio signals in the solar system (see review by Pick & Vilmer 2008).

Sunward of 0.25 au, the variety, occurrence, and amplitude of observed plasma waves in the solar wind all increase compared to 1 au (e.g., Bowen et al. 2020; Malaspina et al. 2020; Mozer et al. 2021a, 2021b; Jagarlamudi et al. 2021). Whistler-mode waves are a notable exception in that they become sparse closer to the Sun (Cattell et al. 2022). One class of wave localized to the near-Sun environment is the electron Bernstein wave, and concurrent similar-frequency waves reported by Malaspina et al. (2020) and explored by Malaspina et al. (2021), Shi et al. (2022), and Tigik et al. (2022). In this paper, these waves are collectively referred to as near-f_{ce} waves, where f_{ce} is the electron cyclotron frequency.

This Letter presents evidence that many of the near-f_{ce} waves reported in the near-Sun solar wind are likely not intrinsic to the free-flowing solar wind. Instead, these waves have properties consistent with generation by interaction of the solar wind plasma and magnetic field with the ion wake of the observing spacecraft. These results build upon the analysis of Tigik et al. (2022), where it was demonstrated that electron Bernstein and similar-frequency waves in the near-Sun solar wind appear when the solar wind magnetic field takes on a narrow range of orientations with respect to the spacecraft–Sun line.

Many prior studies have reported data analysis and/or simulation results demonstrating the generation of plasma waves by interaction between a spacecraft and a flowing plasma (e.g., Keller et al. 1997; Singh 2000; Guio & Pécseli 2005; Endo et al. 2015; Miyake et al. 2020). Some of these studies have specifically identified wake-driven waves near the electron cycltron frequency (Singh 2000; Endo et al. 2015). However, these prior studies were conducted for plasma flows and magnetization conditions significantly different from those encountered by the Parker Solar Probe (PSP).

The results reported here emphasize that interactions between experimental probes and the plasma they seek to measure can manifest in subtle and surprising ways. For that reason, it is important to maintain a scientifically healthy level of skepticism when interpreting plasma wave observations in a newly explored environment.

2. Data

This study makes use of data from the FIELDS (Bale et al. 2016) and SWEAP (Kasper et al. 2016) instruments on the PSP spacecraft (Fox et al. 2016). The FIELDS data used in this study include time-series DC-coupled magnetic field data from the Fluxgate Magnetometer (FGM) and AC-coupled electric field power spectral density data, calculated on board by the Digital Fields Board (DFB) (Malaspina et al. 2016). These power spectra are produced every ~ 1 s, using data from the first $\sim 1/8$ of each second. The SWEAP data used in this study include the proton bulk velocity, determined from moments of the ion distribution functions recorded by the SPANi sensor (Livi et al. 2021). The SWEAP data cadence during the intervals of interest is ~ 7 s.

Data from PSP's fifth and eleventh solar encounter are examined. The perihelion distance reached on these encounters is 27.87 R_S (≈ 0.13 au) and 13.28 R_S (≈ 0.06 au), respectively.

3. Observations

Figure 1 shows data recorded on 2020 June 7. This day, also examined by Tigik et al. (2022), includes the perihelion of PSP's fifth solar encounter (2020 June 7 at 08:19:28 UTC). Figure 1(a) shows time-series FGM data, at ~ 293 samples s^{-1}, in the spacecraft body coordinate system. In this system, $+\hat{z}$ points sunward along the spacecraft–Sun line, $+\hat{x}$ points along
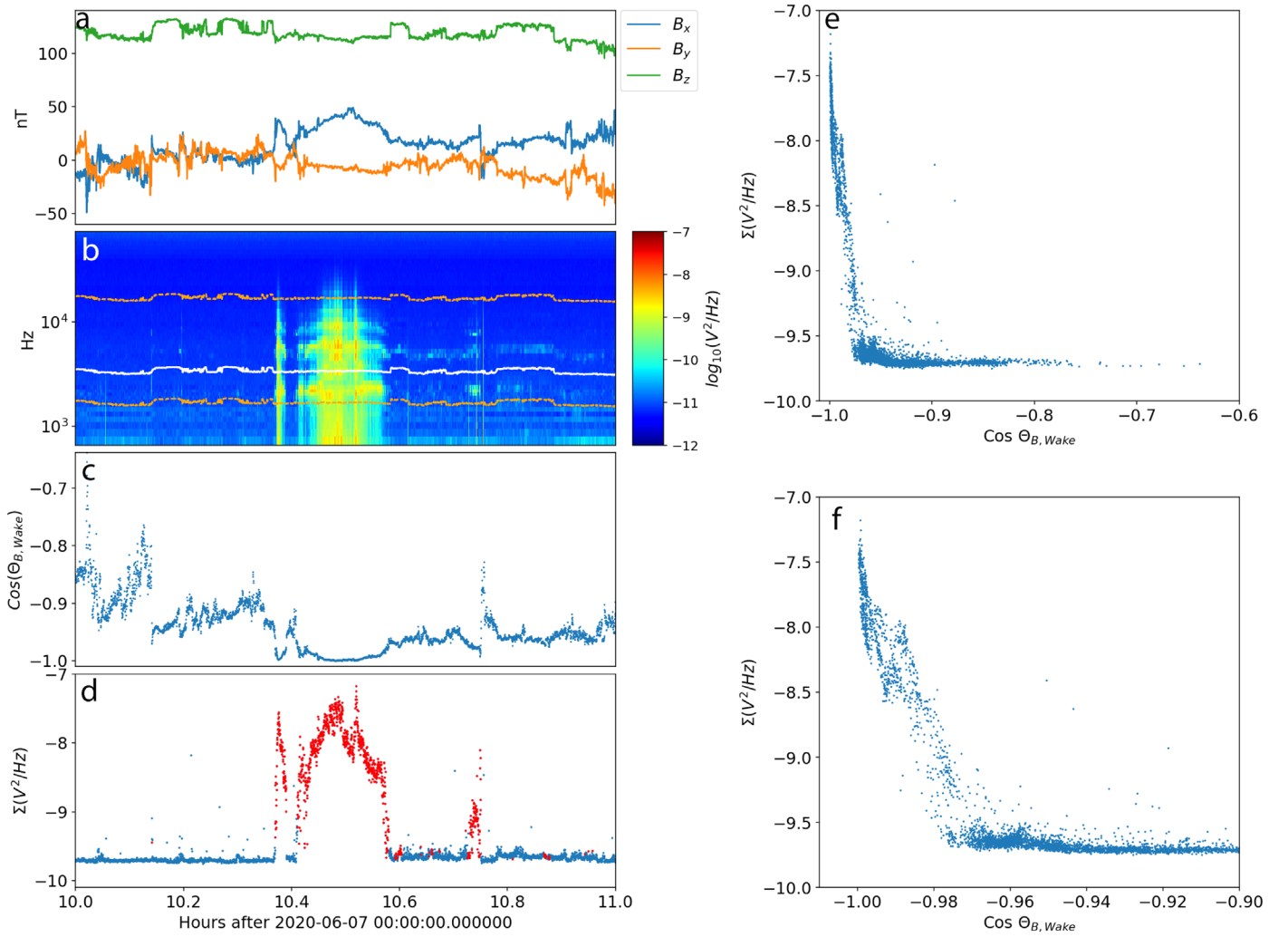
Figure 1. Comparison of near-f_{ce} wave power with alignment between the PSP ion wake direction and the solar wind magnetic field direction. (a) Solar wind magnetic field vector components in spacecraft body coordinates. (b) Electric field power spectral density. The lower orange, white, and upper orange lines indicate $0.5 f_{ce}$, f_{ce}, and $5 f_{ce}$, respectively. (c) The cosine of $\theta_{B,\text{Wake}}$, the angle between the solar wind magnetic field vector and the ion wake direction vector. (d) The integral of the power spectral density in (b) between the frequencies indicated by the two orange lines. (e) Integrated power spectral density as a function of $\theta_{B,\text{Wake}}$. (f) Same as (e), with a narrower range of $\theta_{B,\text{Wake}}$ shown.

the direction of spacecraft motion at perihelion (ram), and $+\hat{y}$ completes the right-handed system, pointing roughly toward ecliptic south. During this time interval, B_z is the largest component, indicating an approximately radial magnetic field. At the center of the interval, B_x increases, and the net magnetic field takes on a Parker spiral-like configuration. At the same time, turbulent fluctuations in B_x, B_y, and B_z all decrease.

Figure 1(b) shows a spectrogram of the differential potential between two antennas in the plane of the heat shield ($\Delta V_{12} = V_1 - V_2$). An intense burst of near-f_{ce} wave power is present at the center of the interval. The white line indicates f_{ce}, while the upper and lower orange lines show $0.5 f_{ce}$ and $5 f_{ce}$, respectively.

Figure 1(c) shows the cosine of the three-dimensional angle between the ambient magnetic field vector and the vector along the spacecraft ion wake direction ($\theta_{B,\text{Wake}}$). The ion wake direction vector is defined as parallel to the ion velocity vector in the spacecraft body frame. Near the center of the time interval, ($\theta_{B,\text{Wake}}$) approaches -1, indicating that the solar wind magnetic field and ion wake vector are anti-parallel.

Figure 1(d) shows the integral of the power spectral density in Figure 1(b) between $0.5 f_{ce}$ and $5 f_{ce}$ at each spectral observation during this interval. Points are plotted in red for spectral samples where $(cos(\theta_{B,\text{Wake}}) < -0.97)$. The vast majority of the near-f_{ce} wave power occurs when the ambient magnetic field is aligned with the ion wake direction.

Both Figures 1(e) and (f) show the integrated power spectral density in Figure 1(d) as a function of $\theta_{B,\text{Wake}}$ (from Figure 1(c)). Figure 1(f) is plotted over a narrower range of $\theta_{B,\text{Wake}}$. From these data, it is evident that nearly all wave power in the near-f_{ce} occurs when when the ambient magnetic field is aligned with the ion wake direction. Also, the wave amplitudes increase as the magnetic field and ion wake vectors become more closely aligned.

Figure 2 has the same format as Figure 1, but covers 11 hours, instead of only one hour, on 2020 June 7. The same patterns noted in Figure 1 are present. More scatter is introduced into the integrated power spectral density because wave modes other than the near-f_{ce} waves are present and contribute to the integration (for example, just before 08:00 UTC). A much broader range of $cos(\theta_{B,\text{Wake}})$ is sampled, but
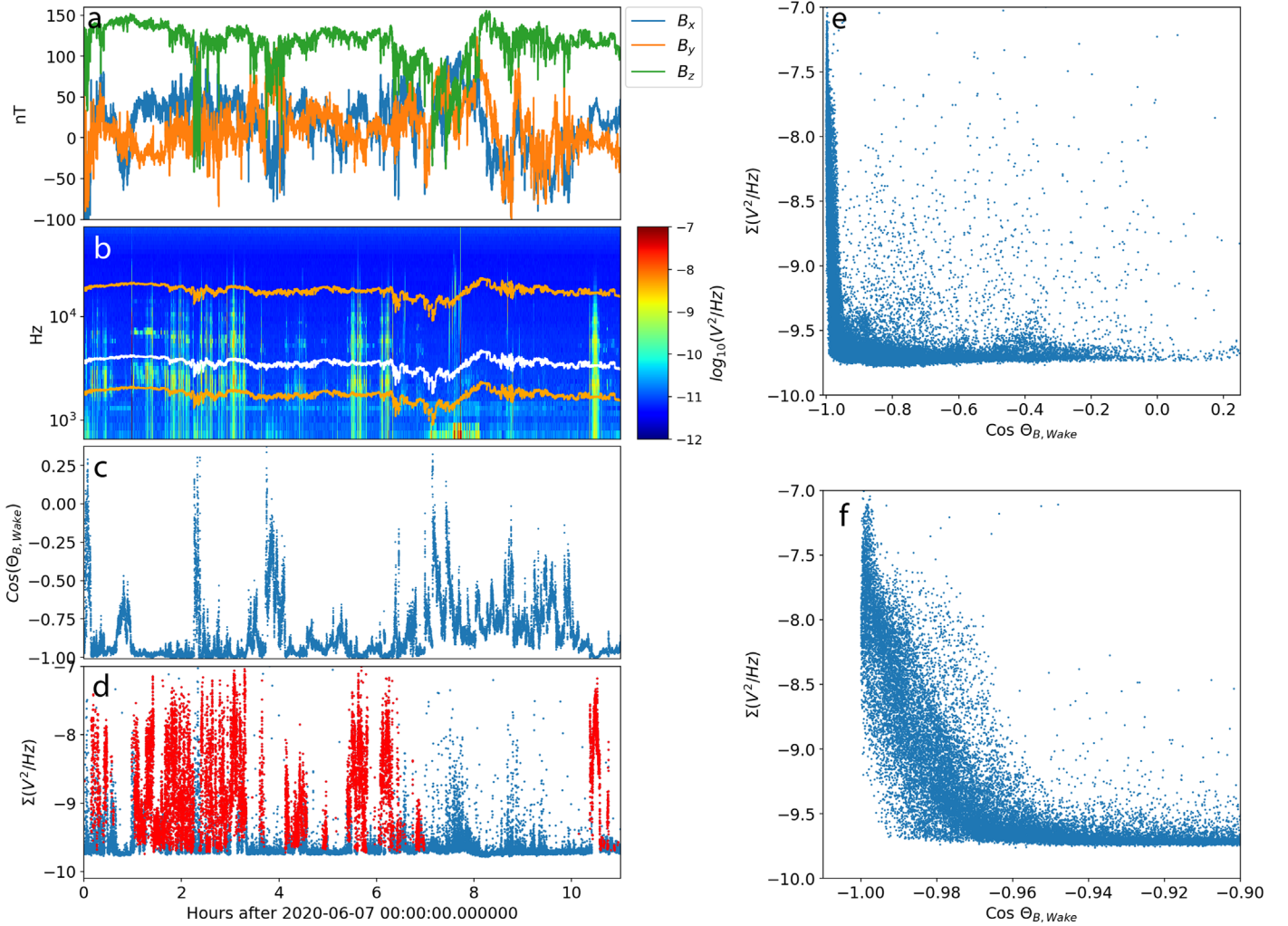
Figure 2. Same format as Figure 1, covering an 11 hr interval on 2020 June 7.

wave power in the near-f_{ce} band continues to appear preferentially, and increase, when the solar wind magnetic field vector becomes anti-parallel with the spacecraft ion wake vector.

Figure 3 has the same format as Figure 1, but covers 24 hr on 2022 February 25. This day contains the perihelion of encounter 11 (at 15:38:04 UTC). This day is chosen because (i) near-f_{ce} waves appear throughout the entire day and (ii) this day contains a heliospheric current sheet crossing, where the magnetic field vector changes direction. Again, the patterns illustrated in Figure 1 persist. Interestingly, the shape of the increase in the near-f_{ce} wave power is not perfectly symmetric between $cos(\theta_{B,\text{Wake}})$ near 1 and $cos(\theta_{B,\text{Wake}})$ near -1. More scatter is present in the data because the spectral signatures of dust impacts and other plasma waves between $0.5 f_{ce}$ and $2 f_{ce}$ are included in the wave power integral.

The events shown are not unique. The near-f_{ce} wave occurrence and amplitude are found to vary with $\theta_{B,\text{Wake}}$ for 20 randomly selected near-f_{ce} wave intervals, each of more than 2 hr in duration, recorded during PSP solar encounters 1 through 12.

4. Discussion

The data presented show that the near-f_{ce} wave power increases as the magnetic field vector direction becomes parallel or anti-parallel with the spacecraft ion wake direction. This strongly supports the Tigik et al. (2022) supposition that interaction between the spacecraft and the solar wind drives near-f_{ce} waves. While this study does not determine the exact mechanism of wave growth, it does place some constraints on possible mechanisms.

The spacecraft creates an ion wake because the ram velocity of solar wind ions, in the spacecraft frame, exceeds the ion thermal velocity, (e.g., Eriksson et al. 2007; Ergun et al. 2010; Miyake et al. 2013). Under these conditions, solar wind ions cannot easily access the ion wake region. Solar wind thermal electrons have thermal energies that significantly exceed the plasma ram velocity, and therefore can access the ion wake region, creating an electrostatically negative region in the ion wake direction. The ion wake extends downstream of the ram velocity of solar wind ions in the spacecraft frame (Ergun et al. 2010).

The spacecraft bus also creates an electron shadow. In near-Sun solar wind plasma conditions, there is a significant fraction of electrons with gyro radii which are on the order of, or smaller than, the spacecraft bus size ($\sim$3 m). These electrons are absorbed by contact with the spacecraft bus. This creates a 'shadow' region along the magnetic field direction that low-energy electrons traveling along the background magnetic field cannot access. For the magnetic field magnitudes in Figures 1,
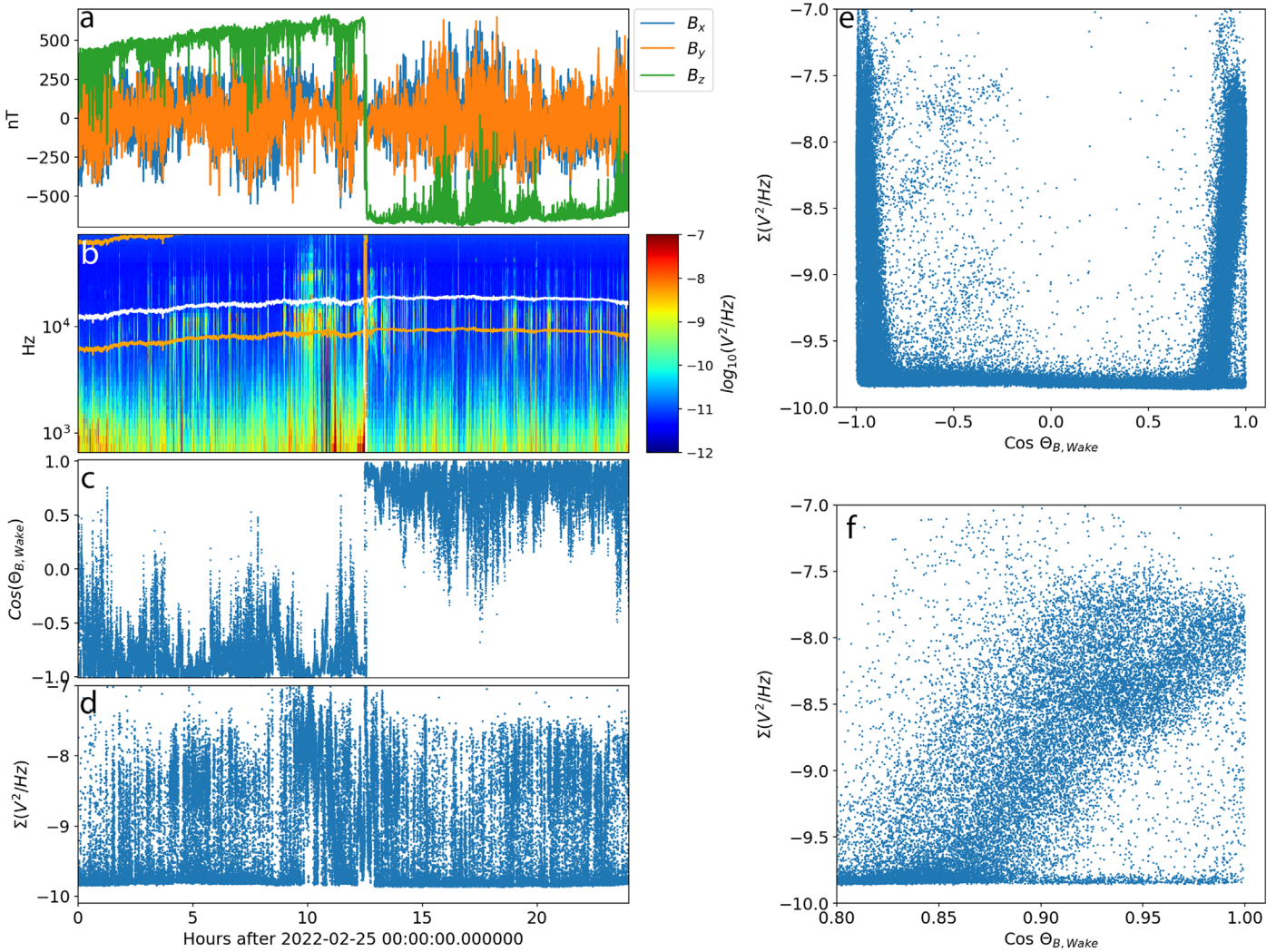
Figure 3. Same format as Figure 1, covering a 24 hr interval on 2022 February 22. For clarity of plotting, red points are not indicated in (d).

2, and 3, an ∼3 m electron gyro radius corresponds to electrons of energies ∼0.012 eV, ∼0.015 eV, and ∼0.3 eV. These energies are well below the energies measurable by the SWEAP electron instruments (Whittlesey et al. 2020), but wake-driven modification of the distribution function can be large enough to allow for the generation of plasma waves.

Prior work (Malaspina et al. 2021) used Doppler shift analysis of near-f_{ce} waves to estimate that they are Landau-resonant with electrons between 0.025 and 0.75 eV, or cyclotron-resonant with electrons between 0.2 and 0.8 eV ($N = 2$ cyclotron resonance). These values are consistent with the energy range for which the PSP spacecraft creates an electron shadow.

The energy of electrons that are shadowed by the PSP spacecraft is proportional to $|B|^2$. Therefore the energy of electrons that can be shadowed by the spacecraft drops rapidly with radial distance, reaching ∼0.001 eV at $|B| \approx 110$ nT, which typically occurs near 0.18 au (Badman et al. 2021). At larger radial distances and weaker magnetic field strengths, the electrons blocked by the spacecraft become a negligible fraction of the total electron velocity distribution. In this circumstance, there are likely to be insufficient electrons to participate in an ion wake/electron shadow wave growth instability. This may explain why near-f_{ce} waves are not

observed outside of 0.25 au (Malaspina et al. 2020). Conversely, as the PSP approaches the Sun, $|B|$ increases, and more electrons in a broader range of energies can participate in an ion wake/electron shadow wave instability. This may explain why near-f_{ce} waves become more prevalent and intense during perihelion passes, such as in encounter 11 (Figure 3).

Both ion wake and electron shadow regions exist for all magnetic field orientations, but the near-f_{ce} waves do not. Near-f_{ce} waves occur when the electron shadow, the direction of which is determined by the magnetic field vector, aligns with the ion wake. When these two regions overlap, solar wind ions from the upstream direction cannot access the ion wake region, and low-energy electrons cannot enter the wake/shadow region from the upstream magnetic field direction.

While detailed simulations are required to determine exact instability mechanisms, it is speculated that the electron shadow creates a gap in the electron velocity distribution function at low energies. This is similar to a one-sided loss cone distribution (e.g., Bingham & Cairns 2000; Lee et al. 2013), but with only low-energy particles absent from the distribution. To produce near-f_{ce} waves when the electron shadow and ion wake overlap, this distribution must be wave-unstable in the absence of solar wind protons. This further

suggests that solar wind protons act to damp wave growth in the electron shadow when it does not align with the ion wake. The one standard deviation width of a $\sim$20 eV proton distribution spans $\sim$0.02 eV in electron energy, consistent with the idea that the solar wind ion distribution may act to damp near-f_{ce} waves when the electron shadow does not align with the ion wake.

5. Conclusions

It was shown that near-f_{ce} waves sunward of 0.25 au observed by the PSP spacecraft occur when (i) the magnetic field direction aligns with the spacecraft ion wake direction and (ii) the ambient magnetic field turbulence is low compared to the typical solar wind (Malaspina et al. 2020; Tigik et al. 2022). Power in these wave modes increases as the magnetic field becomes more closely aligned with the ion wake direction. This behavior demonstrates that interaction of the spacecraft with the ambient plasma and magnetic field is capable of driving near-f_{ce} waves. Therefore, many of the observed waves in this frequency range are not likely to be intrinsic to the free-flowing solar wind.

It is hypothesized that the near-f_{ce} waves grow when the spacecraft ion plasma wake overlaps with the spacecraft electron shadow. Electrons originating from the upstream region along the background magnetic field are excluded from the shadow region when their gyro radii are on the same spatial scale as the spacecraft. The energy of electrons that can be shadowed by the PSP is less than 1 eV, similar to the estimated energy of electrons resonant with near-f_{ce} waves. Because the energy of the unstable electrons is well below what can be measured practically, detailed simulations are required to determine the exact instability mechanism. Finally, the scaling of the spacecraft-shadowed electron energy with the ambient magnetic field strength is consistent with the more frequent observation of these waves closer to the Sun, and non-detection at larger radial distances.

Based on these results, similar near-f_{ce} waves are expected to appear behind other obstacles in the solar wind, such as asteroids or comets, when their electron shadow regions align with their ion wake regions in the presence of a steady ambient magnetic field.

ORCID iDs

David M. Malaspina https://orcid.org/0000-0003-1191-1558
Sabrina F. Tigik https://orcid.org/0000-0002-5968-9637
Andris Vaivads https://orcid.org/0000-0003-1654-841X

References

Badman, S. T., Bale, S. D., Rouillard, A. P., et al. 2021, A&A, 650, A18
Bale, S. D., Goetz, K., Harvey, P. R., et al. 2016, SSRv, 204, 49
Bingham, R., & Cairns, R. A. 2000, PhPl, 7, 3089
Bowen, T. A., Mallet, A., Huang, J., et al. 2020, ApJS, 246, 66
Cattell, C., Breneman, A., Dombeck, J., et al. 2022, ApJL, 924, L33
Endo, K., Kumamoto, A., & Katoh, Y. 2015, JGRA, 120, 5160
Ergun, R. E., Malaspina, D. M., Bale, S. D., et al. 2010, PhPl, 17, 072903
Eriksson, A., Khotyaintsev, Y., & Lindqvist, P.-A. 2007, in Proc. of the 10th Spacecraft Charging Technology Conf., http://www.space.irfu.se/aie/publ/Eriksson2007b.pdf
Fox, N. J., Velli, M. C., Bale, S. D., et al. 2016, SSRv, 204, 7
Guio, P., & Pécseli, H. L. 2005, AnGeo, 23, 853
Jagarlamudi, V. K., Dudok de Wit, T., Froment, C., et al. 2021, A&A, 650, A9
Kasper, J. C., Abiad, R., Austin, G., et al. 2016, SSRv, 204, 131
Keller, A. E., Gurnett, D. A., Kurth, W. S., Yuan, Y., & Bhattacharjee, A. 1997, P&SS, 45, 201
Lee, S.-Y., Yi, S., Lim, D., et al. 2013, JGRA, 118, 7036
Livi, R., Larson, D. E., Kasper, J. C., et al. 2021, Earth Space Sci. Open Arch., doi:10.1002/essoar.10508651.1
Malaspina, D. M., Ergun, R. E., Bolton, M., et al. 2016, JGRA, 121, 5088
Malaspina, D. M., Halekas, J., Bercic, L., et al. 2020, ApJS, 246, 21
Malaspina, D. M., Wilson, L. B. I., Ergun, R. E., et al. 2021, A&A, 650, A97
Miyake, Y., Cully, C. M., Usui, H., & Nakashima, H. 2013, JGRA, 118, 5681
Miyake, Y., Miloch, W. J., Kjus, S. H., & Pécseli, H. L. 2020, JGRA, 125, e27379
Mozer, F. S., Bonnell, J. W., Hanson, E. L. M., Gasque, L. C., & Vasko, I. Y. 2021a, ApJ, 911, 89
Mozer, F. S., Vasko, I. Y., & Verniero, J. L. 2021b, ApJL, 919, L2
Pick, M., & Vilmer, N. 2008, A&ARv, 16, 1
Shi, C., Zhao, J., Malaspina, D. M., et al. 2022, ApJL, 926, L3
Singh, N. 2000, ITPS, 28, 2085
Smith, C. W., & Vasquez, B. J. 2021, FrASS, 7, 114
Tigik, S. F., Vaivads, A., Malaspina, D. M., & Bale, S. D. 2022, ApJ, 936, 7
Vasko, I. Y., Krasnoselskikh, V., Tong, Y., et al. 2019, ApJL, 871, L29
Whittlesey, P. L., Larson, D. E., Kasper, J. C., et al. 2020, ApJS, 246, 74